Available online at www.sciencedirect.com
ScienceDirect
Solar Energy 82 (2008) 80–94
SOLAR ENERGY
www.elsevier.com/locate/solener

Modeling of the optimum tilt of a solar chimney for maximum air flow

E.P. Sakonidou [a,b], T.D. Karapantsios [b,*], A.I. Balouktsis [a], D. Chassapis [a]

[a] Department of Mechanical Engineering, Technological Educational Institution of Serres, End of Magnesia's Str, GR-62100 Serres, Greece
[b] Division of Chemical Technology, Department of Chemistry, Aristotle University of Thessaloniki, University Box 116, GR-54124 Thessaloniki, Greece

Received 18 July 2006; received in revised form 5 February 2007; accepted 6 March 2007
Available online 30 March 2007

Communicated by: Associate Editor S.A. Sherif

Abstract

The aim of this work is to develop a mathematical model to determine the tilt that maximizes natural air flow inside a solar chimney using daily solar irradiance data on a horizontal plane at a site. The model starts by calculating the hourly solar irradiation components (direct, diffuse, ground-reflected) absorbed by the solar chimney of varying tilt and height for a given time (day of the year, hour) and place (latitude). In doing so it computes the transmittance and absorbance of the glazing for the various solar irradiation components and for various tilts. The model predicts the temperature and velocity of the air inside the chimney as well as the temperatures of the glazing and the black painted absorber. Comparisons of the model predictions with CFD calculations delineate the usefulness of the model. In addition, there is a good agreement between theoretical predictions and experiments performed with a 1 m long solar chimney at different tilt positions.

Keywords: Solar chimney; Chimney effect; Natural ventilation; Solar air heater; Tilt; Maximum flow

1. Introduction

Solar chimneys differ from conventional chimneys in that their southern wall (for the north hemisphere) is replaced by a transparent sheet, i.e. glazing, that allows the collection and use of solar irradiation. Many works, especially the last two decades, have illustrated the advantages in using solar chimneys accounting also for their low maintenance cost and superb durability. Solar chimneys have been traditionally used in agriculture for air renewal in barns, silos, greenhouses, etc. as well as in drying of crops, grains, fruits or wood (e.g. Garg, 1987; Das and Kumar, 1989; Ekechukwu and Norton, 1995; Vlachos et al., 2002). Another popular application is for natural ventilation in buildings in order to improve the quality of indoors air and increase the comfort index for inhabitants (e.g. Kumar et al., 1998; Ziskind et al., 2002; Ding et al., 2004, 2005; Bansal et al., 2005). Having in mind climatization and energy conservation in buildings, efforts have also been made to evaluate the performance of special chimney configurations, such as solar roof collectors and Trombe-walls (e.g. Gan, 1998; Sànchez et al., 2003; Ong and Chow, 2003; Khedari et al., 2000, 2003; Heras et al., 2005) as well as other hybrid constructions involving inclined, vertical or horizontal heated walls with cooling cavities (e.g. Raman et al., 2001; Jiang and Chen, 2003; Kazansky et al., 2003; Dai et al., 2003).

Most published works deal with solar chimneys fixed at a specific inclination, usually vertical, as these are easier to construct and operate. To overcome the diurnal variability of solar irradiance, some of them used heating elements to maintain either uniform wall temperature or wall heat flux and examined only the heat transfer and fluid mechanics performance of the chimney (e.g. Bouchair and Fitzgerald, 1988; Bouchair, 1994; Moshfegh and Sandberg, 1998; Afonso and Oliveira, 2000; Chen et al., 2003). These studies

* Corresponding author. Tel.: +30 2310997772; fax: +30 2310997759.
E-mail address: karapant@chem.auth.gr (T.D. Karapantsios).

0038-092X/$ - see front matter © 2007 Elsevier Ltd. All rights reserved.
doi:10.1016/j.solener.2007.03.001

Nomenclature

Latin symbols

a	absorptance
A	surface area
C_d	discharge coefficient
c_p	specific heat
d	depth of the chimney gap
D_H	hydraulic diameter of the chimney
f	wall friction coefficient
G_{sc}	solar constant (1367 W/m^2)
h	convective heat transfer coefficient
hour	hour of the day
H	daily irradiation on a horizontal plane
H_{ch}	height difference between outlet and inlet of the chimney
H_0	daily extraterrestrial irradiation on a horizontal plane
I	hourly irradiation on a horizontal plane
K	extinction coefficient of the glass
k_{in} and k_{out}	inlet and outlet pressure loss coefficients
k_T	clearness index
ℓ	path length of irradiation through the glass
L	length of the chimney
n	day of the year (1 to 365)
Nu	Nusselt number
r	ratio of the hourly irradiation over the daily irradiation
r_g	diffuse reflectance of the surroundings
$r_\perp$	perpendicular component of unpolarized irradiation
$r_\parallel$	parallel component of unpolarized irradiation
R_b	ratio of the direct irradiation on a tilted plane over that on the horizontal plane
Ra	Rayleigh number
Ra_c	critical Rayleigh number
Re	apparent Reynolds number
s	slope of the chimney with respect to the horizontal plane
T	temperature
U	overall heat transfer coefficient
w	width of the chimney gap

Greek symbols

α and β	coefficients in Eq. (9)
δ	declination (angular position of the sun at solar noon)
ε	emmitance of the black wall
η_1 and η_2	refraction indexes of air and glass, respectively
θ	angle
θ_1	angle of irradiation incidence
θ_2	angle of refraction
λ	thermal conductivity of air
μ	viscosity
ρ	density
σ	Stefan-Boltzmann constant ($= 5.6697 \times 10^{-8}$ W/m^2 K^4)
τ	glass transmittance,
τ_r	average of $r_\perp$ and $r_\parallel$
υ	average air velocity inside the chimney
ϕ	latitude of the site (angular distance from the equator)
ω	hour angle

Subscripts

α	absorber
αbs	absorption
air	air
bw	black wall
dif	diffuse
dir	direct
g	glazing
gap	chimney gap
0	ambient conditions
ref	reflection
s	sunset
T	tilted plane

showed that there are distinctly different flow patterns between narrow and wide chimney gaps and that the ratio of chimney length/gap influences the air flow rate.

Awbi and Gan (1992) obtained analytically the air temperature and flow rate profiles along a Trombe wall, considering a uniform wall temperature. The same authors employed also CFD codes to simulate the air flow and heat transfer in a chimney of varying gap width (for large gaps 3D simulations were indispensable). Both analytical and numerical results were in good agreement with earlier data. Bansal et al. (1993) developed a steady state analytical model for uniform wall temperature applied to a solar system consisting of a solar air heater connected to a conventional chimney. Andersen (1995) derived a set of equations to predict the natural ventilation in a room with small openings based on the pressure model. Gan (1998) and Gan and Riffat (1998) used 3D CFD techniques to study the parameters that influence the performance of a Trombe wall. An interesting result of these studies was that ventilation rates increased along with the thickness of the interior wall. Moshfegh and Sandberg (1998), investigated air movement behind photovoltaic panels using a 2D CFD code coupled with a standard k–ε turbulence model and a wall function. Their predictions of air velocity and temperature distributions were in accord with their experimental results. A similar 2D CFD approach was also adopted by Rodrigues et al. (2000) who provided detailed calculations of the velocity and temperature profiles in the chimney.

Using the concept of a thermal resistance network, Ong and Chow (2003) developed an analytical model to examine the effects of air gap and solar irradiation intensity on the performance of different chimneys assuming uniform heat flux on the heated wall. Many of the above studies provided evidence that for chimneys with gap-to-length ratio less than or close to 1:10, the temperature can be assumed uniform across the chimney gap and so 2D models can give reasonably accurate predictions.

Solar chimneys employing inclined collectors can evidently exploit more the incident irradiation to enhance air flow in the chimney. As the inclination of the chimney varies, two things occur that work in opposite directions with respect to the air flow rate. A higher inclination results in a higher exposure of the wall to solar irradiation and hence yield higher heat utilization and more intense buoyant airflow. On the other hand, tilting the chimney reduces the effective pressure head of the chimney and so diminishes air flow. It is apparent that there must be an optimum tilt that leads to the highest flow rate, compromising these two effects. Although there are e few studies coping with the effect of inclination on a chimney performance, they usually involve heating means other than solar irradiance to achieve uniform wall heat flux (e.g. Moshfegh and Sandberg, 1998; Chen et al., 2003) and so a parametric analysis with respect to the temporal variability of solar irradiation is not possible.

To our knowledge, there are only two earlier studies that examined systematically the effect of inclination for chimneys where the absorbed heat flux depends on the diurnal and seasonal variations of solar irradiation. The first is the work by Prasad and Chandra (1990) who performed numerical calculations and also did experiments for a solar chimney 1.5 m long and with 20 mm gap width. Their model, though detailed for the momentum and heat transfer in the fluid, had certain drawbacks: did not account for heat losses, required knowledge of the ratio of diffuse/total irradiation and, finally, assumed that the transmittance of the glazing and absorptance of the black wall were unity although it is known that these quantities vary with inclination (Duffie and Beckman, 1991). The agreement between predictions and experiments was rather poor but their finding that the optimum tilt for maximum irradiance uptake (i.e. maximum air temperature), is distinctly different than the optimum tilt for maximum air velocity in the chimney was significant. They calculated optimum tilt angles for maximum air velocity to oscillate periodically throughout the year between a low value, 52°, in summer months and a high value, 72°, in winter months (for Calcutta, India). A much simpler treatment of solar irradiation and glazing optical properties was employed by Hamdy and Fikry (1998) for Alexandria (Egypt) and summer months. For these particular conditions, an optimum tilt around 60° was estimated for maximum air flow.

Data of solar irradiation at a site that are easily accessible by a design engineer usually refer to monthly average daily values of total irradiation on a horizontal plane, e.g. ELOT (1991). Therefore for designing a solar chimney, horizontal irradiation data have first to be transformed to irradiation data at a slope. For accurate estimations, it is important to base the design on hourly values of solar irradiation which must then be determined from the available daily values. In any case, it is necessary to decompose the total irradiation arriving at the sloped surface into its major components (direct, diffuse and ground-reflected) since for each of them the optical properties (transmittance and absorptance) of the glass cover varies differently with the tilt. As far as we know, there is no prior work that deals with the estimation of the optimum tilt of a solar chimney for maximizing air flow starting from data of daily total solar irradiation on an horizontal plane and taking into account all the above considerations. It is indeed the scope of this study to propose an engineering model that can cope with this task. The term engineering denotes a simplified model adequate for design purposes and field applications which does not employ detailed 2D/3D fluid mechanics and heat transfer calculations.

In the following, the setup of the engineering and CFD models is presented first. Next, the solar chimney construction and operation are outlined. Finally, theoretical predictions from the models are compared and discussed against each other and against experimental results.

2. Theory

2.1. Engineering model

In the analysis below, it is assumed that the incident solar irradiation is sufficient to bring the chimney's body to its steady state temperature. The input data to the model are divided in five categories: (a) chronological (day of the year, hour) and geographical (latitude), (b) meteorological (monthly average daily total irradiation on an horizontal plane, monthly average daily ambient temperature), (c) geometrical (dimensions of chimney, thicknesses of glazing and insulation material), (d) optical/irradiation properties of the construction materials (refractive index and extinction coefficient of the glazing, absorptance and emmitance of the black surfaces), and (e) physical properties of air and insulation materials for calculating heat losses. The chimney tilt and length are treated as variables in the range 30–90° (angles from the horizontal plane) and 1–12 m, respectively. Physical properties of air are taken from VDI-Wärmeatlas (1991). Data for monthly average daily total irradiation and monthly average ambient temperature are taken from ELOT (1991) – the Greek Organization of Standardization – for Serres, a city in North Greece where also the experimental tests are performed. The ELOT data agree reasonably well with measurements from the meteorological station of TEI – Serres with only a ~3% annual deviation (Karapantsios et al., 1999).

The model consists of three basic subroutines. The first one estimates the solar irradiation components (direct, diffuse and ground-reflected) that hit the surface of the

chimney on an hourly basis, at varying tilt and length. For this calculation, only the chronological, geographical and meteorological information mentioned above is needed. The relations below, unless differently stated, are taken from Duffie and Beckman (1991).

The total daily irradiation on a horizontal plane, H, is customary expressed as the sum of two components: the direct (beam) irradiation and the diffuse irradiation from the sky

$$H = H_{\mathrm{dir}} + H_{\mathrm{dif}} \tag{1}$$

The daily extraterrestrial solar irradiation H_0 on a horizontal plane is given as

$$H_0 = \frac{24 \times 3600}{\pi} G_{\mathrm{sc}} \left(1 + 0.033 \cos \frac{360n}{365}\right) \times \left[\cos\phi \cos\delta \sin\omega_{\mathrm{s}} + \frac{\pi\omega_{\mathrm{s}}}{180} \sin\phi \sin\delta\right] \tag{2}$$

where G_{sc} is the solar constant (1367 W/m^2), n is the day of the year (1–365), ϕ is the latitude of the site (angular distance from the equator, for Serres $\phi = 41$), δ is the declination (angular position of the sun at solar noon) and ω_{s} is the sunset hour angle given as

$$\omega_{\mathrm{s}} = \arccos(-\tan\phi \tan\delta) \tag{3}$$

The declination δ is found from the equation:

$$\delta = 23.45 \sin\left(360 \frac{284 + n}{365}\right) \tag{4}$$

The daily extraterrestrial solar irradiation H_0 is related with the daily total irradiation H (input variable to the code), via the clearness index k_{T}:

$$k_{\mathrm{T}} = \frac{H}{H_0} \tag{5}$$

Knowing the value of the clearness index, one can calculate the diffuse component, H_{dif}, as follows for $\omega_{\mathrm{s}} \leqslant 81.4°$:

$$\frac{H_{\mathrm{dif}}}{H} = \begin{cases} 1.0 - 0.2727k_{\mathrm{T}} + 2.4495k_{\mathrm{T}}^2 \\ \quad -11.9514k_{\mathrm{T}}^3 + 9.3879k_{\mathrm{T}}^4 \quad \text{for} \quad k_{\mathrm{T}} < 0.715 \\ 0.143 \quad \text{for } k_{\mathrm{T}} \geqslant 0.715 \end{cases} \tag{6}$$

whereas for $\omega_{\mathrm{s}} > 81.4°$

$$\frac{H_{\mathrm{dif}}}{H} = \begin{cases} 1.0 + 0.2832k_{\mathrm{T}} - 2.5557k_{\mathrm{T}}^2 + 0.8448k_{\mathrm{T}}^3 \\ \quad \text{for } k_{\mathrm{T}} < 0.722 \\ 0.143 \quad \text{for } k_{\mathrm{T}} \geqslant 0.722 \end{cases} \tag{7}$$

Then, the direct daily component can be computed from Eq. (1). The ratio of the total hourly irradiation, I, over the total daily irradiation, H, is given by

$$r_t = \frac{I}{H} \tag{8}$$

and can be found from the relation

$$r_t = \frac{\pi}{24}(\alpha + \beta\cos\omega) \frac{\cos\omega - \cos\omega_{\mathrm{s}}}{\sin\omega_{\mathrm{s}} - \frac{\pi\omega_{\mathrm{s}}}{180}\cos\omega_{\mathrm{s}}} \tag{9}$$

where the coefficients α and β are given by

$$\alpha = 0.409 + 0.5016 \sin(\omega_{\mathrm{s}} - 60) \tag{10}$$

$$\beta = 0.6609 - 0.4767 \sin(\omega_{\mathrm{s}} - 60) \tag{11}$$

and the hour angle ω that appears above is given by

$$\omega = (hour - 12) * \frac{360}{24} \tag{12}$$

where *hour* denotes the hour of the day (input variable). Likewise, the ratio of the hourly diffuse irradiation, I_{dif}, over the daily diffuse irradiation, H_{dif}, is given as

$$r_{\mathrm{dif}} = \frac{I_{\mathrm{dif}}}{H_{\mathrm{dif}}} \tag{13}$$

where

$$r_{\mathrm{dif}} = \frac{\pi}{24} \frac{\cos\omega - \cos\omega_{\mathrm{s}}}{\sin\omega_{\mathrm{s}} - \frac{\pi\omega_{\mathrm{s}}}{180}\cos\omega_{\mathrm{s}}} \tag{14}$$

Then, I and I_{dif} are calculated from Eqs. (8) and (13), respectively, whereas the hourly direct irradiation, I_{dir}, is computed as

$$I_{\mathrm{dir}} = I - I_{\mathrm{dif}} \tag{15}$$

A customary approach for irradiation estimations on sloped surfaces is to consider an isotropic 2D model for the diffuse irradiation (Liu and Jordan, 1963) and also assume that the reflecting surfaces are diffuse and not specular reflectors. Recent studies, (e.g. Badescu, 2002) have shown that isotropic 3D models perform better than the Liu–Jordan isotropic 2D model which seems to overestimate the diffuse and underestimate the ground reflected solar irradiation component, respectively. For sites around our latitude or smaller, the diffuse and reflected components are usually much less than the direct solar irradiation component. In addition, for the most common chimneys inclinations (close to vertical) the differences between 2D and 3D models diminish and, therefore, can be safely ignored. For these reasons the present calculations utilize the well-known Liu–Jordan isotropic 2D model. In this case, the total irradiation on a surface tilted at slope s, is given by Sukhatme (1984)

$$I_{\mathrm{T}} = I_{\mathrm{dir}} R_{\mathrm{b}} + I_{\mathrm{dif}} \left(\frac{1 + \cos s}{2}\right) + I r_{\mathrm{g}} \left(\frac{1 - \cos s}{2}\right) \tag{16}$$

On the RHS of Eq. (16), the first term represents the direct component, the second term the diffuse component and the third term the component that is reflected from the surroundings. In (16), r_{g} is the diffuse reflectance of the surroundings (usually around 0.25) and R_{b} is the ratio of direct irradiation on the tilted surface over that on the horizontal plane. R_{b} for the northern hemisphere is given by Sukhatme (1984):

$$R_{\mathrm{b}} = \frac{\cos(\phi - s)\cos\delta\cos\omega + \sin(\phi - s)\sin\delta}{\cos\phi\cos\delta\cos\omega + \sin\phi\sin\delta} \tag{17}$$

Thus, the average hourly irradiation components on a tilted surface that enter in the calculations of the solar chimney are

$$I_{T,dir} = I_{dir} \cdot R_b \tag{18}$$

$$I_{T,dif} = I_{dif} \cdot \left(\frac{1+\cos s}{2}\right) \tag{19}$$

$$I_{T,ref} = I \cdot 0.25 \cdot \left(\frac{1-\cos s}{2}\right) \tag{20}$$

The second subroutine of the model evaluates the transmittance, τ, and absorptance, a_g, of the glazing for the various components of the incident solar irradiation. The transmittance for the direct irradiation component, τ_{dir}, is approximately given by the product:

$$\tau_{dir} \cong \tau_{\alpha bs,dir} \cdot \tau_{ref,dir} \tag{21}$$

where $\tau_{\alpha bs,dir}$ denotes the ratio of the transmitted versus the incident irradiation where only absorption losses have been considered and $\tau_{ref,dir}$ denotes the transmittance of initially unpolarized irradiation where only reflection losses have been considered.

In Eq. (21), $\tau_{\alpha bs,dir}$ is given as

$$\tau_{\alpha bs,dir} = \exp\left(-\frac{K\ell}{\cos\theta_2}\right) \tag{22}$$

where K is the extinction coefficient of the glass that varies from approximately $4\ m^{-1}$ for "water white" glass to approximately $32\ m^{-1}$ for poor (greenish cast of edge) glass (Duffie and Beckman, 1991). In this work, $K = 10\ m^{-1}$. Moreover, ℓ designates the path length of irradiation through the glass which in effect is the thickness of the glass. In this work, $\ell = 0.004$ m. Finally, θ_2 is the angle of refraction, which is calculated from the expression:

$$\frac{\eta_1}{\eta_2} = \frac{\sin\theta_1}{\sin\theta_2} \tag{23}$$

where η_1 and η_2 are the refraction indexes of air and glass, respectively; in this work, $\eta_1 = 1$ and $\eta_2 = 1.526$ (Duffie and Beckman, 1991). Furthermore, θ_1 is the angle of incidence calculated as

$$\theta_1 = \arccos\left[\sin(\phi - s)\sin\delta + \cos(\phi - s)\cos\delta\cos\omega\right] \tag{24}$$

The parameter τ_r is the average of two components

$$\tau_{r,dir} = \frac{1}{2}\left(\frac{1-r_\parallel}{1+r_\parallel} + \frac{1-r_\perp}{1+r_\perp}\right) \tag{25}$$

where $r_\perp$ represents the perpendicular component and $r_\parallel$ the parallel component of unpolarized irradiation given by

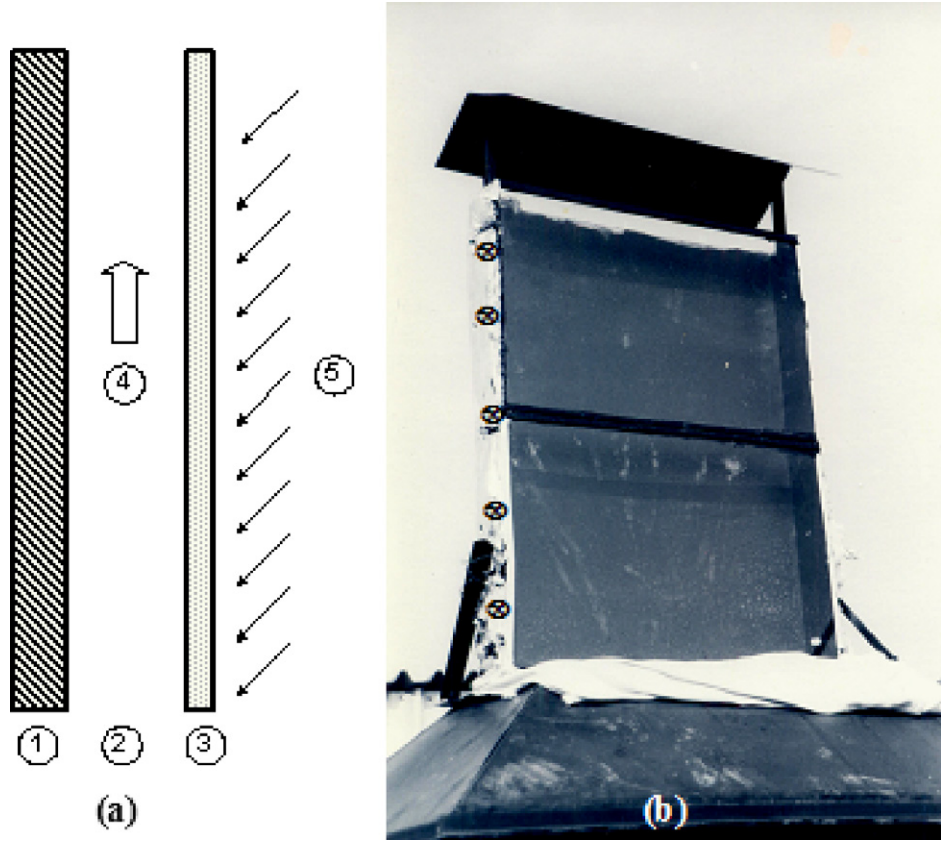

Fig. 1. Solar chimney configuration. (a) schematic of the cross-section of a solar chimney showing critical elements, 1: insulated black-painted absorber, 2: air entry, 3: glazing, 4: air flow direction, 5: incident irradiation and (b) photo of the chimney employed in the experiments (⊗: measuring station).

$$r_{\perp} = \frac{\sin^2(\theta_2 - \theta_1)}{\sin^2(\theta_2 + \theta_1)} \quad (26)$$

$$r_{\parallel} = \frac{\tan^2(\theta_2 - \theta_1)}{\tan^2(\theta_2 + \theta_1)} \quad (27)$$

The diffusion component, τ_{dif}, and the refection component, τ_{ref}, of the glass transmittance, are calculated in the same manner as τ_{dir} but with the slope s in Eq. (24) replaced by the diffusion angle, θ_{dif}, and the reflection angle, θ_{ref}, respectively, defined as

$$\theta_{dif} = 59.7 - 0.1388 \cdot s + 0.001497 \cdot s^2 \quad (28)$$

and

$$\theta_{ref} = 90 - 0.5788 \cdot s + 0.002693 \cdot s^2 \quad (29)$$

Accordingly, the components of the glass absorptance: direct, $a_{g,dir}$, diffuse, $a_{g,dif}$ and reflected, $a_{g,ref}$, are given by the following approximate relations:

$$a_{g,dir} \cong 1 - \tau_{\alpha bs,dir} \quad (30)$$

$$a_{g,dif} \cong 1 - \tau_{\alpha bs,dif} \quad (31)$$

$$a_{g,ref} \cong 1 - \tau_{\alpha bs,ref} \quad (32)$$

For conciseness, the products $(\tau \cdot I)_T$ and $(a_g \cdot I)_T$ will henceforth denote the following quantities:

$$(\tau \cdot I)_T = \tau_{dir} \cdot I_{T,dir} + \tau_{dif} \cdot I_{T,dif} + \tau_{ref} \cdot I_{T,ref} \quad (33)$$

$$(a_g \cdot I)_T = a_{g,dir} \cdot I_{T,dir} + a_{g,dif} \cdot I_{T,dif} + a_{g,ref} \cdot I_{T,ref} \quad (34)$$

These are quantities that appear in the heat balance equations of the chimney and therefore need be evaluated first when running the code.

The third subroutine of the model solves the overall energy balance of the chimney in the form of a system of three algebraic equations describing the heat exchange across the black wall (absorber), the glazing and the air inside the chimney, respectively. Fig. 1a shows a schematic representation of the solar chimney configuration including most critical elements. The heat exchange equations are (temperatures in Kelvin)

$$a_{bw}(\tau \cdot I)_T A_g = U_{bw} \cdot A_{bw} \cdot (T_{bw} - T_0) + h_{bw} \cdot A_{bw} \cdot (T_{bw} - T_{air}) + \varepsilon \cdot \sigma \cdot A_g \cdot (T_{bw}^4 - T_g^4) \quad (35)$$

$$(a_g \cdot I)_T A_g + \varepsilon \cdot \sigma \cdot A_g \cdot (T_{bw}^4 - T_g^4) = h_g \cdot A_g \cdot (T_g - T_{air}) + U_g \cdot A_g \cdot (T_g - T_0) \quad (36)$$

$$h_{bw} \cdot A_{bw} \cdot (T_g - T_{air}) + h_g \cdot A_g \cdot (T_g - T_{air}) = 2 \cdot c_{p,air} \cdot \rho_{air} \cdot A_{gap} \cdot \upsilon \cdot (T_{air} - T_0) \quad (37)$$

In these equations, the three unknowns are T_{bw} the average temperature of the black wall, T_{air} the average air temperature in the chimney and T_g the average glass temperature. T_0, is the ambient temperature which is an input variable. Moreover, A_{bw} is the surface area of the black wall, A_g is the surface area of the glass cover and A_{gap} is the cross sectional area of the chimney gap. Furthermore, U_{bw} is the overall heat transfer coefficient between the black wall and the surroundings (in this work, $U_{bw} = 0.9$ W/m^2 K for a typical insulation thickness of 5 cm with thermal conductivity of 0.045 W/m K and moderate ambient conditions), U_g is the overall heat transfer coefficient between the glass cover and the surroundings (in this work, $U_g = 9$ W/m^2 K chosen from the range 1–15 W/m^2 K proposed by Garg, 1987), h_{bw} is the convective heat transfer coefficient between the black wall and the air in the chimney and h_g is the convective heat transfer coefficient between the glass cover and the air in the chimney. In addition, a_{bw} is the absorptance of the black wall (in this work, $a_{bw} = 0.9$, a value chosen from Duffie and Beckman, 1991), ε is the emmitance of the black wall (in this work, $\varepsilon = 0.95$, a value chosen from Duffie and Beckman, 1991). Also, σ is the Stefan-Boltzmann constant ($= 5.6697 \times 10^{-8}$ W/m^2 K^4) whereas $c_{p,air}$ and ρ_{air} are the temperature dependent specific heat and density of air, respectively. Finally, υ is the average air velocity along the chimney which since it can not stand as a fourth unknown in the above system of equations it must be described by some relation based on the other parameters of the system (see below).

The convective heat transfer coefficients for both the glass cover and the black wall and strictly for the vertical position of the chimney are given by the relation (VDI-Wärmeatlas, 1991):

$$Nu_{g,bw} = \frac{h_{g,bw} L}{\lambda} = \left\{0.825 + 0.387 \cdot \left(0.345 \cdot Ra_{g,bw}\right)^{1/6}\right\}^2 \quad \text{for } 10^{-1} < Ra\sin(s) < 10^{12} \quad (38)$$

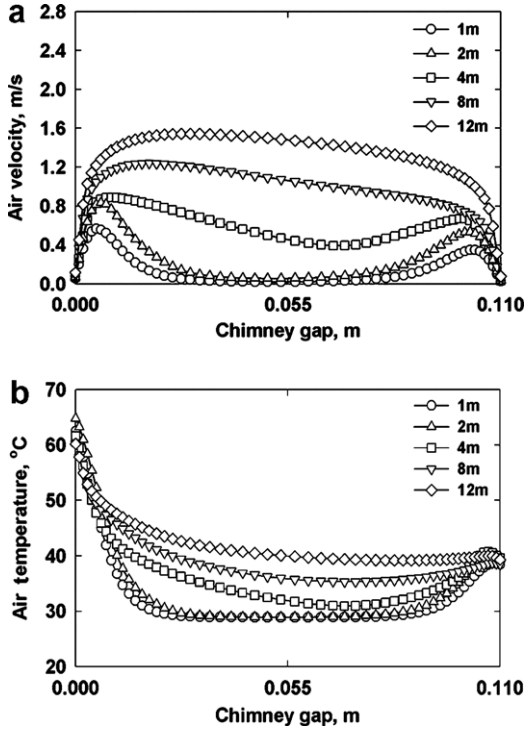

Fig. 2. Air velocity profile (a) and air temperature profile (b) across the chimney gap for different chimney lengths at the vertical position as calculated by the CFD model (day = 196, $H = 23.1$ MJ/m^2, $T_{amb} = 28.9$ °C).

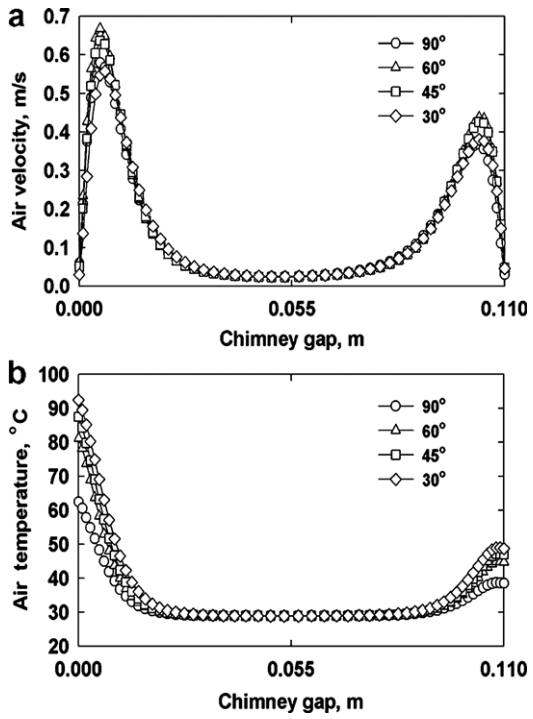

Fig. 3. Air velocity profile (a) and air temperature profile (b), across the chimney gap for different tilt angles for a chimney of 1m length as calculated by the CFD model (day = 196, $H = 23.1$ MJ/m^2, $T_{amb} = 28.9$ °C).

In the above, Nu is the Nusselt number, Ra is the Rayleigh number, L is the length of the chimney and λ is the thermal conductivity of air. For inclinations between 30° and 75°, the heat transfer coefficient for the glass cover h_g (heated surface facing downwards) and the black wall h_{bw} (heated surface facing upwards) are calculated from the relations (VDI-Wärmeatlas, 1991):

$$Nu_g = \frac{h_g L}{\lambda} = 0.56[Ra_g \sin(s)]^{1/4} \quad \text{for } 10^5 < Ra\sin(s) < 10^{11} \tag{39}$$

$$Nu_{bw} = \frac{h_{bw} L}{\lambda} = 0.56[Ra_c \sin(s)]^{1/4} + 0.13[Ra^{1/3} - Ra_c^{1/3}] \quad \text{for } 10^8 < Ra\sin(s) < 10^{11} \tag{40}$$

where Ra_c is a critical Rayleigh number that designates the transition between laminar and turbulent flow and which is given approximately by

$$\log(Ra_c) = 8.9 - 0.00178 \cdot (90 - s)^{1.82} \tag{41}$$

Eqs. (39) and (40) were originally obtained from experiments with inclinations below 75°. For this, for inclinations between 75° and 90°, cubic spline interpolation is employed to achieve smooth variation of coefficients with inclination.

In order to describe the average air velocity inside the chimney as a function of other system parameters, two different expressions have been tried. The first one is derived

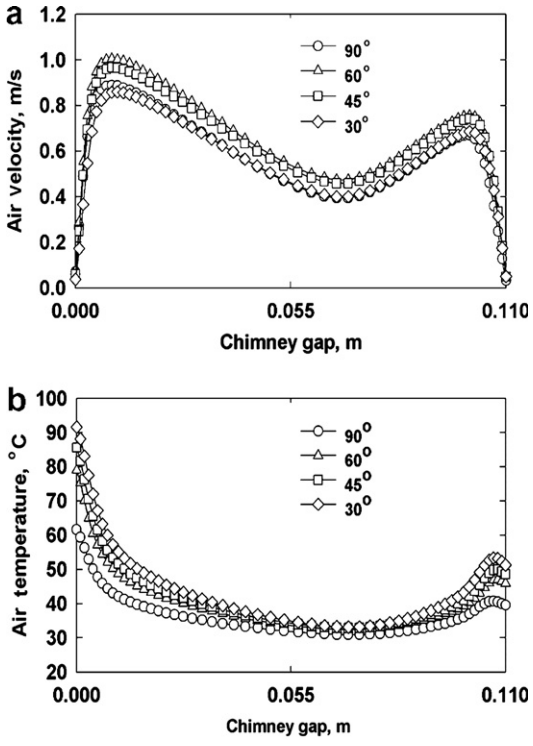

Fig. 4. Air velocity profile (a) and air temperature profile (b), across the chimney gap for different tilt angles for a chimney of 4 m length as calculated by the CFD model (day = 196, $H = 23.1$ MJ/m^2, $T_{amb} = 28.9$ °C).

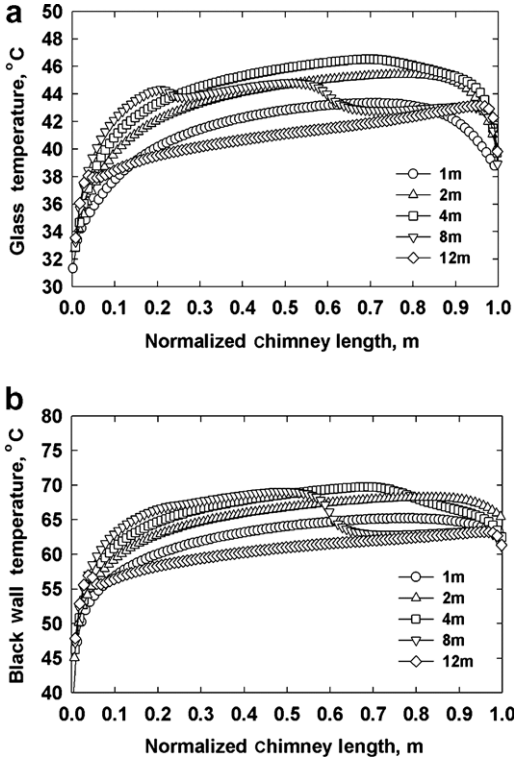

Fig. 5. Temperature of glazing (a) and absorber wall (b) along the normalized chimney length for different chimney lengths at the vertical position as calculated with the CFD model (day = 196, $H = 23.1$ MJ/m^2, $T_{amb} = 28.9$ °C).

by assuming that the pressure head inside a tilted chimney counterbalances completely the pressure drop due to the wall friction and inlet and outlet pressure losses. For equal cross sectional areas at the inlet and outlet of the chimney and for small density differences along the chimney this yields:

$$f \cdot \frac{L}{D_H} \cdot \frac{\rho_{air} v^2}{2} + k_{in} \cdot \frac{\rho_{air} v^2}{2} + k_{out} \cdot \frac{\rho_{air} v^2}{2} = H_{ch} \cdot g \cdot \sin(s) \cdot (\rho_0 - \rho_{air}) \quad (42)$$

where D_H is the hydraulic diameter of the chimney defined as

$$D_H = \frac{2 \cdot w \cdot d}{w + d} \quad (43)$$

w is the width of the chimney gap and d is the depth of the chimney gap. Also, k_{in} and k_{out} are the inlet and outlet pressure loss coefficients, H_{ch} is the height difference between outlet and inlet of the chimney ($= L \cdot \sin(s)$) and f is the wall friction coefficient calculated (for turbulent flow) as

$$f = \frac{0.316}{Re^{1/4}} \quad (44)$$

where Re is the apparent Reynolds number, defined as $D_H v \rho_{air}/\mu_{air}$. Combining the above yields:

$$v = \left[\frac{2 \cdot L \cdot g (\sin(s))^2 (\rho_0 - \rho_{air})}{\left(f \cdot \frac{L}{D_H} + k_{in} + k_{out} \right) \cdot \rho_{air}} \right]^{1/2} \quad (45)$$

For a rectangular channel with both ends open and heated on one wall, Sandberg and Moshfegh (1998), proposed $k_{in} = 1.5$, $k_{out} = 1.0$ and $f = 0.056$.

The second expression that has been tried in the model was described by Bansal et al. (1993) and Andersen (1995). This is an empirical relation which uses the concept of a discharge coefficient to adjust the air velocity for the total flow resistances in the system (friction losses along the chimney wall, inlet and outlet pressure losses, etc). For a case of equal cross sectional areas at the inlet and outlet of the chimney this relation reduces to (T in Kelvin):

$$v = C_d \cdot \frac{\rho(T_{air})}{\rho(T_0)} \cdot \left[\frac{L \cdot g \cdot (\sin(s))^2 \cdot (T_{air} - T_0)}{T_0} \right]^{1/2} \quad (46)$$

where C_d is the discharge coefficient which for thermal buoyant flows was proposed as 0.57 (Andersen, 1995).

2.2. CFD model

The commercial CFD code Fluent 6.1.18 is employed to simulate and check the heat transfer and fluid mechanics parts of the engineering model. For this, the CFD model uses as input data – apart from the chimney dimensions and material properties – the output data of the first two subroutines of the model, that is, the values of the total irradiation absorbed by the black wall and the glass cover.

Given the narrow geometry of our chimney (gap-to-length ratio 1:10), a 2D CFD model is considered adequate based on the assumption of uniform temperature distributions across the chimney width. The employed geometrical domain has a variable length (1–12 m) as the first dimension and a fixed gap depth (0.11 m) as the second one. The third dimension (width = 0.74 m) is used only for estimation of total flow rates. The computational grid is a pure map mesh with the cells clustered towards the black wall and the glass. The grid for the 1 m high chimney consists of 500 cells along the chimney and 55 cells across the gap (27,500 quad cells in total), with an average size of 2 mm. For the taller chimneys the grid size is increased proportionally in the length dimension to maintain the same spatial resolution.

Preliminary simulations showed that there are conditions where transition from laminar to turbulent flow occurs within the chimney and therefore, simulations are performed with both the laminar and turbulent models. For the latter, the shear-stress transport (SST) k–ω model with the transitional flows option active is used (Fluent user's guide, 2003), which is suitable for low Reynolds turbulent flows. This model combines the traditional two-layer turbulent zonal model with enhanced wall functions. A fine mesh close to the walls is created with $y+ \approx 2$, to completely resolve the viscosity affected near-wall region.

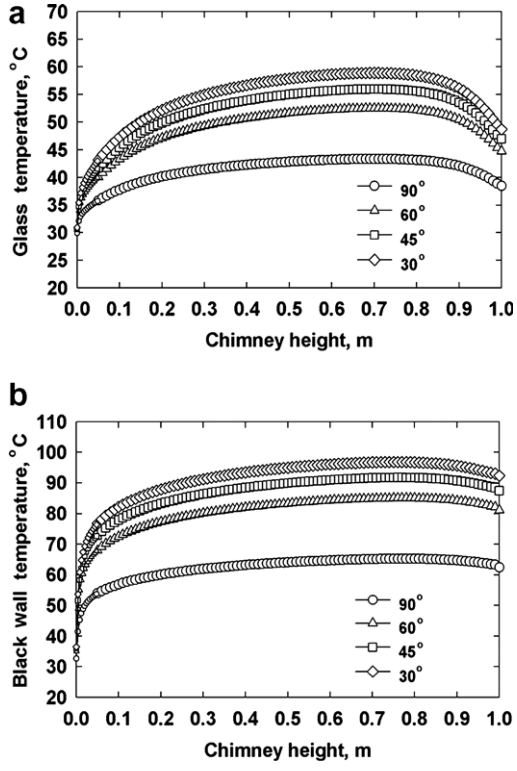

Fig. 6. Temperature of glazing (a) and absorber wall (b) along the normalized chimney length for different chimney tilt angles for a chimney of 1 m length as calculated with the CFD model (day = 196, $H = 23.1$ MJ/m^2, $T_{amb} = 28.9$ °C).

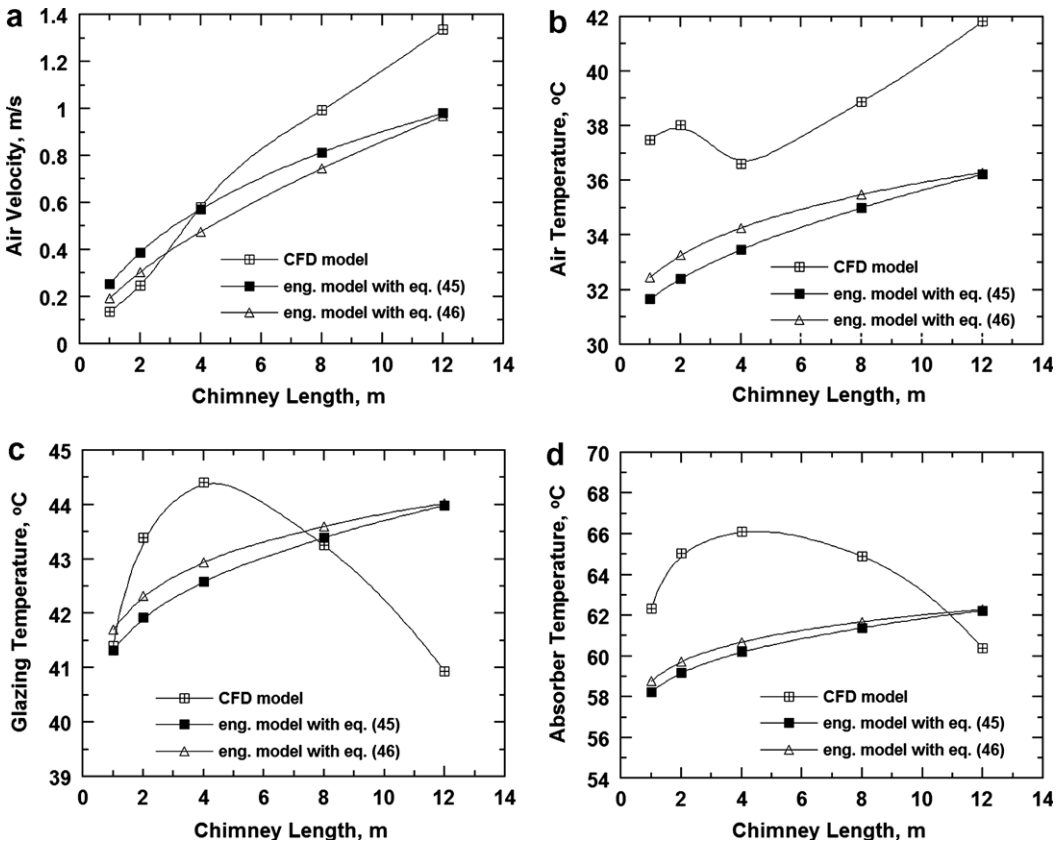

Fig. 7. Average air velocity (a), average air temperature (b), average glazing temperature (c) and average absorber temperature (d) versus chimney length at the vertical position as calculated by two versions of the engineering model and the CFD code (day = 196, $H = 23.1$ MJ/m^2, $T_{amb} = 28.9$ °C).

The energy equation is employed to model the heat transfer phenomena with the Boussinesq approximation to hold for the density of air. Irradiation modeling is implemented using the Surface-to-Surface model (Fluent user's guide, 2003), which accounts for the irradiation exchange in an enclosure of gray-diffuse surfaces. The imposed boundary conditions for the two chimney walls, (glazing and absorbing black wall) are that they both have zero slip and internal emmitance of 0.95.

3. Experiment

The experimental chimney duct has the shape of a narrow parallelepiped with dimensions: 1 m height, 0.74 m width and 0.11 m gap. Black painted aluminum sheet (1.5 mm thick) is used for the construction of the rear and side walls of the chimney. These walls have high solar absorptance (~0.95) and low long wave emittance (~0.05) (Garg, 1987). A 5 cm thick fiberglass layer ($\lambda = 0.045$ W/m K) is the outside insulation material of these walls. The chimney's front side (glazing) is a commercial glass, 3 mm thick. The chimney glazing has a south orientation at all times.

In order the chimney to stand at various inclinations, it is mantled onto a short (0.5 m) metallic trapezoid equipped with special fittings that allow the chimney to lie at different tilt positions. Special care is given to make the chimney light enough so that it can be stably supported by the trapezoid when tilted and so permit easy handling of measuring probes. Even so, for slopes less than 45° it was difficult to hold the chimney firmly.

Along the two vertical narrow side walls of the parallelepiped's section (1×0.11 m), five holes are drilled to facilitate the insertion of measuring probes at distances 0.14 m, 0.34 m, 0.54 m, 0.75 m and 0.89 m from the bottom of the chimney, respectively. Special contact-type thermocouples (K type, OMEGA Inc.) are employed to measure the surface temperature of the glazing and the black wall at three positions across the chimney width (left, center, right) to check for 3D effects. From the recorded data, average values are presented from those three positions since the variance (= SD/average) is less than 0.05. Fig. 1b shows a photo of the constructed solar chimney where the five measuring stations along the vertical side wall are indicated.

Efforts have been made to measure the velocity of the air in the chimney with a hot-wire anemometer probe furnished with sensitive temperature sensors (DO 2003, DELTA OHM). Unfortunately, due to the low height of the chimney, the measured velocities were always below 0.2 m/s. For such low velocities – although within the measuring range of the anemometer – the readings were very unstable perhaps due to minor atmospheric disturbances. So, comparisons with theoretical predictions are based on temperature measurements. This shortcoming is partly alle-

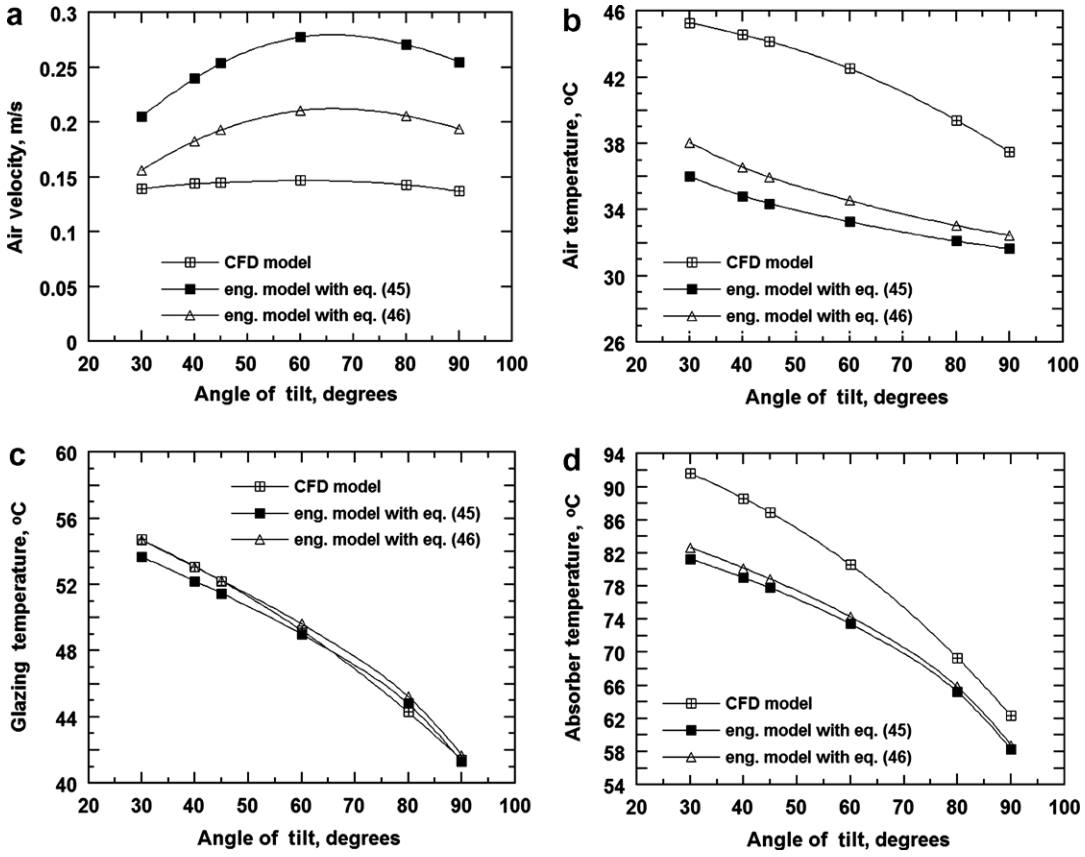

Fig. 8. Average air velocity (a), average air temperature (b), average glazing temperature (c) and average absorber temperature (d) versus chimney tilt for a chimney of 1 m length as calculated by two versions of the engineering model and the CFD code (day = 196, $H = 23.1$ MJ/m^2, $T_{amb} = 28.9$ °C).

viated by the fact that with such a low height (i.e., lightweight) chimney it was possible to use it at different inclinations, an issue essential for this work.

Total horizontal irradiation data are collected and integrated over 10 min intervals, for the period of the experiments with an Eppley Precision Pyranometer (model PSP). The experiments are performed in Serres, Greece (latitude 41°07′, longitude 23°34′, altitude 32 m).

4. Results and discussion

4.1. CFD parametric study

It is illustrative to display first the CFD calculations in order to appreciate the velocity and temperature profiles in the chimney and their variation with respect to height and tilt. Due to space limitations only simulations at a summer day are presented: day 196 (mid July), monthly average daily total irradiation on a horizontal plane 23.1 MJ/m^2 and monthly average daily ambient temperature 28.9 °C. These data are taken for the city of Serres from ELOT (1991).

Fig. 2a shows the air velocity profile across the chimney gap at the exit of a vertical chimney, with chimney length as a parameter. The shape of the velocity profiles for the two smaller lengths (1 and 2 m) are typical of non-interacting boundary layers flowing past the absorber wall (gap position = 0) and the glazing (gap position = 0.11), respectively. Two local maxima are observed near these walls (the higher for the hotter absorber wall) whereas at the centre of the chimney the velocity is close to zero. So, it is not so strange that we were not able to measure significant air velocities in our 1 m chimney. The situation changes for higher chimneys where the two boundary layers start to interact leading to less pronounced local maxima and a smoother velocity front with appreciable velocities at the center of the chimney. The overall air velocity (and therefore air flow rate) increases significantly with chimney length due to the higher pressure head but also higher difference between inside air temperature and ambient temperature. Above 4 m, full pipe flow prevails which, yet, is not symmetrical across the gap. Inspection of the CFD results (not shown due to space limitations) shows a transition from laminar to turbulent flow for higher than ~3 m chimneys.

Fig. 2b displays the corresponding mass-weighted – "cup-mixing" – air temperature profiles. Mass-weighted temperature values depict better the energy content of air which affects the flow rate. As expected, the higher air temperatures are near the black absorber wall which seems to be the main heat supplier of the system. Again, for 1 m and 2 m chimneys the two boundary layers hardly sense each

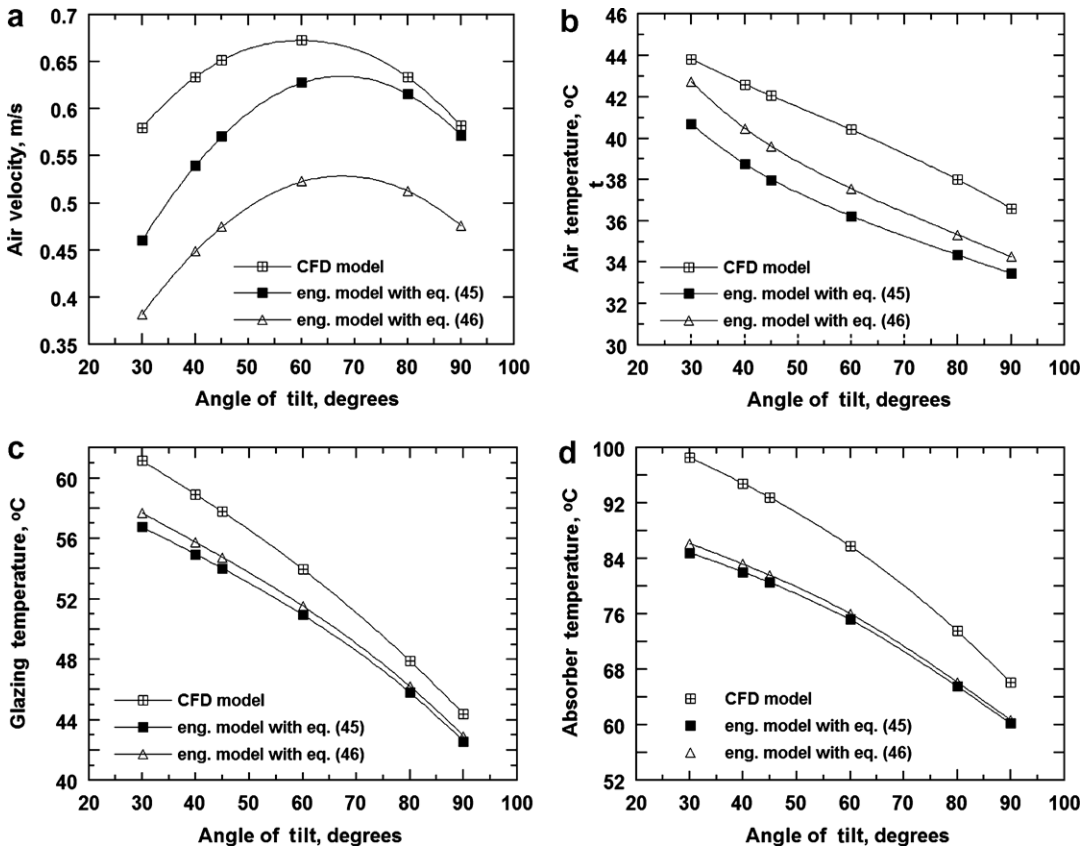

Fig. 9. Average air velocity (a), average air temperature (b), average glazing temperature (c) and average absorber temperature (d) versus chimney tilt for a chimney of 4 m length as calculated by two versions of the engineering model and the CFD code (day = 196, $H = 23.1$ MJ/m^2, $T_{amb} = 28.9$ °C).

other; the temperatures at the center of the gap being very close to the incoming ambient temperature. This, changes drastically for chimneys above 4 m. For the latter, an interesting change of the slope of the profiles occurs near the glazing as a result of temperature mass-weighting.

Figs. 3 and 4 show the influence of the tilt position on (a) air velocity and (b) mass-weighted air temperature across the chimney gap for chimney lengths 1 m and 4 m, respectively. The main features of both the velocity and temperature profiles are essentially those described in Fig. 2 and do not seem to vary with tilt. For both chimneys, it is clear that the higher velocities are achieved at 60° whereas the higher temperatures at 30°. In addition, the air temperature in contact with the walls for the vertical chimney is appreciably lower than the values for the other angles but this is not so for the velocity. Both the above findings manifest a different influence of tilt on heat transfer and fluid flow in the chimney with the consequence that the maximum energy uptake not to coincide with the maximum air flow rate.

The influence of chimney length on (a) the glazing temperature and (b) the absorber temperature is shown in Fig. 5 for an inclination of 90°. Normalization in the length scale is performed by division with the total chimney length. Qualitatively speaking, the two walls exhibit similar trends. However, the absorber is always warmer than the glazing at the same length. Both walls are heated up significantly within a very short distance from the inlet of the chimney since there velocities are low and so energy cannot be promptly transferred to the air stream. A bit upstream where the walls are already warm, their temperature increases more gradually because both the air velocity and the temperature difference ($T_{wall} - T_{air}$) driving the heat transfer towards the air become significant. Near the top of the chimney, radiation losses come into play and reduce the temperature of the walls. It is interesting that for chimneys between 1 and 4 m length, the local temperature of the walls increases with length. On the contrary, for higher chimneys the local temperature of the walls decreases with length. This may be attributed to full pipe turbulent flow that starts to develop for chimneys above ~3 m. When this happens, the heat transfer coefficient increases and so the walls are cooled down. The same transition phenomena most probably explain also the stepwise drop of temperature midway the 8 m chimney. For even higher chimneys, e.g. 12 m, the wall temperatures increase almost linearly with height indicating a pretty constant turbulent field.

Fig. 6 illustrates the influence of the tilt angle on (a) the glazing temperature and (b) the absorber temperature for a chimney of 1 m length. As can be seen, the local temperatures get higher as the tilt gets lower, for both walls. This is

qualitatively what has been also observed in Fig. 3b regarding the air temperature and demonstrates that there is a direct relationship between the thermal condition of the walls and that of air. If one further considers Fig. 3a, it is apparent that in solar chimneys the tilt for maximum absorbed irradiation does not coincide with the tilt for maximum air flow.

4.2. Comparison between CFD and engineering models

Fig. 7a–d compares CFD predictions with predictions from the engineering model, as a function of chimney length for a vertical orientation of the chimney. Predictions refer to average air velocity and air temperature in the chimney as well as average glazing temperature and absorber temperature. Two series of model predictions are presented; one based on Eq. (45) and the other on Eq. (46) for the estimation of air velocity in the chimney. Results only for day 196 (mid July) are presented since this proved to be the most stringent period for comparisons with the largest deviations between models. In all four plots, it is apparent that the two versions of the engineering model give comparable results. Yet, they are different from the CFD results. Regarding air velocity, CFD data are lower than the engineering model data for chimneys less than 2 m but the situation reverses for chimneys above 4 m. Air temperatures predicted by the engineering model are below the values predicted by the CFD code for all the examined lengths. Interestingly, CFD results show a non-monotonous sigmoid behavior with a kink point around 4 m. This is most likely due to the prevailing turbulent conditions for chimneys longer than 4 m. A non-monotonous behavior is also observed in the CFD predictions of the glazing and absorber temperatures with a peak value again close to 4 m. The latter means that for chimneys taller than 4 meters heat transfer from the walls to the flowing air is drastically enhanced, indicating once more turbulent flow conditions.

Figs. 8a–d and 9a–d show the dependence of all model predictions on the angle of the tilt for chimney lengths 1 m and 4 m, respectively. Calculations are again for day 198 (mid-July) where comparisons among models are less favorable. Despite the deviations among models in the predicted values of air velocity, air temperature, glazing temperature and absorber temperature, there is a good agreement on the optimum tilt that yields maximum air velocity: The engineering model predicts an optimum tilt around 65° whereas the CFD code around 60°. This result has great significance as it lends support to the use of the simpler engineering model for preliminary design purposes and for comparisons between cases.

4.3. Comparison between predictions and experiments

Next, the CFD and the engineering model predictions are compared against experimental measurements. The days for conducting the experiments were carefully selected for wind speed to be less than 0.5 m/s. Runs were performed at days 305, 306 and 307 (beginning of November). The values of total horizontal irradiation and ambient temperature mentioned in the Figure captions are those measured on the spot and used as inputs to the models. It must be stressed in advance that for November the deviations between CFD and engineering model predictions are much less than for July (worst case).

Fig. 10a compares the predicted glazing and absorber temperatures to measured values for a vertical position of the chimney. Error bars denote the standard deviation of measurements. During the measuring period the ambient temperature was not constant so two series of CFD data were calculated based on two different values for the ambient temperature. The first one is the average temperature and the second one the median temperature of the measuring period. As can be seen, the experimental data agree reasonably well with predictions. Fig. 10b displays comparisons regarding the average air temperature. There is again a fair agreement between data and predictions. This is even more so if one considers that measurements may be a bit higher than in reality due to the irradiation absorbed by the finite size measuring probe (part of the

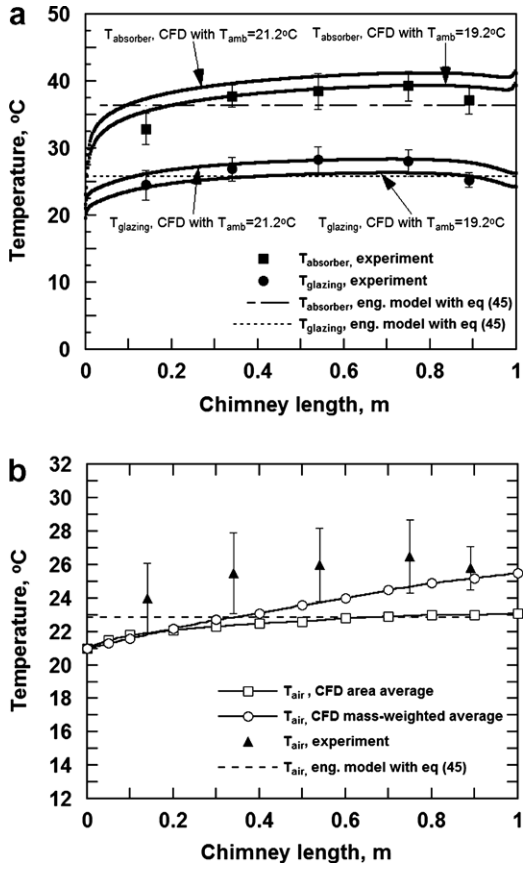

Fig. 10. Comparison between the engineering model predictions against CFD and experimental results as regards (a) the temperatures of the glazing and the absorber and (b) the air temperature along the chimney length. Plot (a): day = 307, $H = 8.12\ \mathrm{MJ/m^2}$, median $T_{amb} = 19.2\ ^\circ\mathrm{C}$, average $T_{amb} = 21.2\ ^\circ\mathrm{C}$. Plot (b): day = 307, $H = 8.12\ \mathrm{MJ/m^2}$, average $T_{amb} = 21.2\ ^\circ\mathrm{C}$.

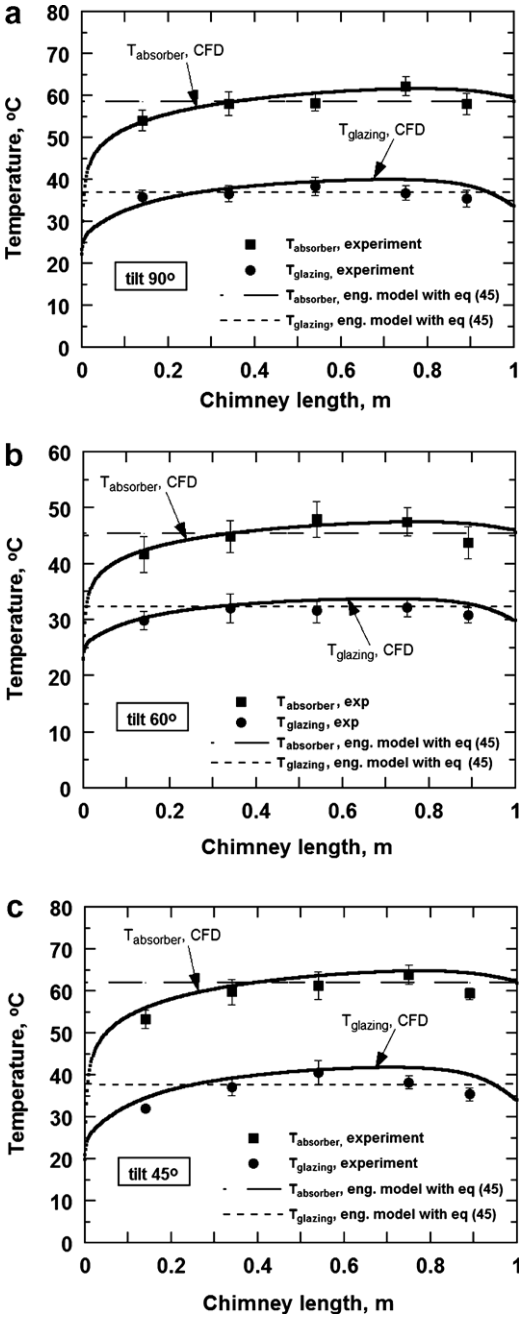

Fig. 11. Comparison between the engineering model predictions against CFD and experimental results as regards the temperatures of the glazing and the absorber along the chimney length (a) for 90°, (b) 60° and (c) 45° angle of tilt. Plot (a): day = 305, $H = 9.70$ MJ/m^2, $T_{amb} = 21.7$ °C. Plot (b): day = 305, $H = 9.05$ MJ/m^2, $T_{amb} = 19.1$ °C. Plot (c): day = 306, $H = 9.90$ MJ/m^2, $T_{amb} = 23.1$ °C.

hot wire probe). Fig. 11a–c shows comparisons for the chimney placed on the trapezoid base and fixed at three different inclinations. Again the agreement between predictions and measurements is good.

4.4. Chimney tilt for maximum air flow

Calculations with the engineering model (using Eq. (45)) for the different months of the year to identify the optimum tilt yielding maximum air flow are presented next, Fig. 12a. The input values of monthly average daily total irradiation on a horizontal plane and monthly average daily ambient temperature, are taken from ELOT (1991). The corresponding maximum velocity values are also displayed to allow appraisal of changes throughout the year. For comparison, Fig. 12b shows the tilt that yields maximum absorbed irradiation along with the corresponding irradiation values on the horizontal plane.

Clearly, air velocity and total irradiation optimum tilts exhibit similar trends receiving their lower values during summer months. However, the angles themselves are very different. So, for maximum air flow the chimney tilt varies in a rather narrow range between 65° and 76° whereas for maximum irradiation it varies between 12° and 44°. Furthermore, the variation of irradiation values throughout the year is much larger (on a percentage basis) than the variation of velocity values. In the relevant work of Prasad and Chandra (1990), conducted for a location in India, qualitatively similar trends were observed but the range of the angles was different: between 53° and 76° for maximum air flow and between 0° and 55° for maximum irradiation.

The question now arises on what is the best choice for the tilt if the chimney is to be fixed at one and only inclina-

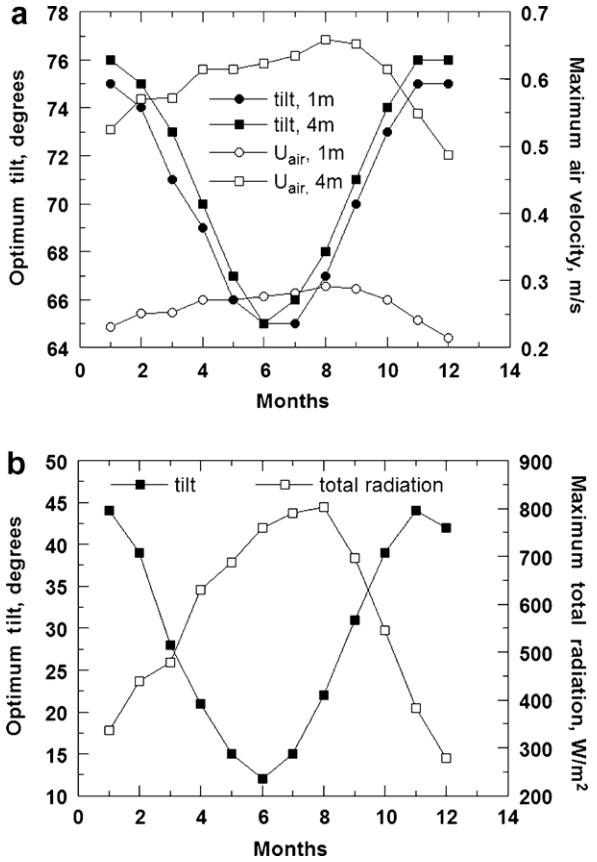

Fig. 12. (a) Optimum tilt and corresponding maximum air velocity (for a 1 m and a 4 m chimney) and (b) optimum tilt and corresponding maximum total irradiation (for any chimney length) versus month of the year as calculated by the engineering model.

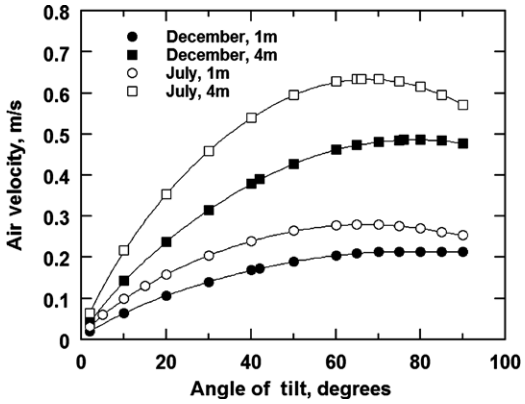

Fig. 13. Average air velocity versus chimney tilt for a 1 m and a 4 m chimney as calculated by the engineering model for the mid day of December and July.

tion throughout the year. To help answer this, Fig. 13 displays the air velocity versus the tilt for a 1 m and a 4 m chimney and for the midday of December and July. Evidently, for winter applications the slight increase (~1%) in air velocity by using the optimum tilt (as compared to a vertical chimney) is not worth it against concerns about the stability of the construction. However, during summer months the gain in air velocity for the optimum tilt is around 10% and decisions must be made more carefully.

5. Conclusion

A composite engineering model is developed that estimates the tilt of a solar chimney that yields the largest natural air flow through it. The model starts by calculating the solar energy absorbed by the solar chimney of varying tilt and height for a given time (day of the year, hour) and place (latitude). The monthly average daily value of total irradiance and the ambient temperature are required as inputs to the code along with some information on the dimensions and properties of the construction materials (absorber, glazing, insulation). The outputs of the model are the velocity and temperature of the air inside the chimney and the temperatures of the glazing and the black painted absorber, as a function of tilt and height. Comparisons of the model predictions with CFD results for a broad range of chimney lengths (1–12 m) and tilts (30–90°) delineates the usefulness of the model but marks also its limitations. Moreover, model predictions are in satisfactory accord with experimental measurements from a 1 m chimney operated at different inclinations. The reasonable agreement between model predictions with CFD and experimental results encourages the use of the engineering model as a tool for evaluating design parameters and for comparative studies.

Acknowledgements

The project is co-funded by the European Social Fund and National Resources – (EPEAEK-II) ARHIMIDIS. The authors are indebted to Mr. N. Vallous for his editorial work.

References

Afonso, C., Oliveira, A., 2000. Solar chimneys: simulation and experiment. Energy and Buildings 32, 71–79.
Andersen, K.T., 1995. Theoretical considerations on natural ventilation by thermal buoyancy. ASHRAE Transactions 101 (2), 1103–1117.
Awbi, H.B., Gan, G., 1992. Simulation of solar-induced ventilation. In: Proceedings of the Second World Renewable Energy Congress (WREC '92), vol. 4, Reading, UK, pp. 2016–2030.
Badescu, V., 2002. 3D approximation for solar diffuse irradiance on tilted surfaces. Renewable Energy 26, 221–233.
Bansal, N.K., Mathur, R., Bhandari, M.S., 1993. Solar chimney for enhanced stack ventilation. Building and Environment 28, 373–377.
Bansal, N.K., Mathur, J., Mathur, S., Jain, M., 2005. Modeling of window-sized solar chimneys for ventilation. Building and Environment 40, 1302–1308.
Bouchair, A., 1994. Solar chimney for promoting cooling and ventilation in Southern Algeria. Building Service Engineering Research Technology 15 (2), 81–93.
Bouchair, A., Fitzgerald, D., 1988. The optimum azimuth for a solar chimney in hot climates. Energy and Buildings 12, 135–140.
Chen, Z.D., Bandopadhayay, P., Halldorsson, J., Byrjalsen, C., Heiselberg, P., Li, Y., 2003. An experimental investigation of a solar chimney model with uniform wall heat flux. Building and Environment 38, 893–906.
Dai, Y.J., Sumathy, K., Wang, R.Z., Li, Y.G., 2003. Enhancement of natural ventilation in a solar house with a solar chimney and a solid adsorption cooling cavity. Solar Energy 74, 65–75.
Das, S.K., Kumar, Y., 1989. Design and performance of a solar dryer with vertical collector chimney suitable for rural application. Energy Conversion Management 29 (2), 129–135.
Ding, W., Minegishi, Y., Hasemi, Y., Yamada, T., 2004. Smoke control based on a solar-assisted natural ventilation system. Building and Environment 39, 775–782.
Ding, W., Hasemi, Y., Yamada, T., 2005. Natural ventilation performance of a double-skin façade with a solar chimney. Energy and Buildings 37, 411–418.
Duffie, J.A., Beckman, W.A., 1991. Solar Engineering of Thermal Processes, second ed. Wiley-Interscience, New York, pp. 3–146.
Ekechukwu, O.V., Norton, B., 1995. Design and measured performance of a solar chimney for natural circulation solar energy dryers. Journal of Solar Energy Engineering 118, 69–71.
ELOT, 1991. Greek Bureau of Standards No. 1291.
Fluent user's guide, 2003. Fluent Inc.
Gan, G., 1998. A parametric study of Trombe walls for passive cooling of buildings. Energy and Buildings 27, 37–43.
Gan, G., Riffat, S.B., 1998. A numerical study of solar chimney for natural ventilation of buildings with heat recovery. Applied Thermal Engineering 18, 1171–1187.
Garg, H.P., 1987. Solar food drying. In: Advances in Solar Energy Technology Collection and Storage Systems, vol. 1. D. Reidel Publishing Co., Dordrecht, pp. 1–123.
Hamdy, I.F., Fikry, M.A., 1998. Passive solar ventilation. Renewable Energy 14, 381–386.
Heras, M.R., Jiménez, M.J., San Isidro, M.J., Zarzalejo, L.F., Pérez, M., 2005. Energetic analysis of a passive solar design, incorporated in a courtyard after refurbishment, using an innovative cover component based in a sawtooth roof concept. Solar Energy 78, 85–96.
Jiang, Y., Chen, Q., 2003. Buoyancy-driven single-sided natural ventilation in buildings with large openings. International Journal of Heat and Mass Transfer 46, 973–988.
Karapantsios, T.D., Hatzimoisiadis, K.A., Balouktsis, A.I., 1999. Estimation of total atmospheric pollution using global irradiation data: introduction of a novel clear day selection methodology. Renewable Energy 17, 169–181.

Kazansky, S., Dubovsky, V., Ziskind, G., Letan, R., 2003. Chimney-enhanced natural convection from a vertical plate: experiments and numerical calculations. International Journal of Heat and Mass Transfer 46, 497–512.

Khedari, J., Boonsri, B., Hirunlabh, J., 2000. Ventilation impact of a solar chimney on indoor temperature fluctuation and air change in a school building. Energy and Buildings 32, 89–93.

Khedari, J., Rachapradit, N., Hirunlabh, J., 2003. Field study of performance of solar chimney with air-conditioned building. Energy 28, 1099–1114.

Kumar, S., Sinha, S., Kumar, N., 1998. Experimental investigation of a solar chimney assisted bioclimatic architecture. Energy Conversion Management 39, 441–444.

Liu, B.Y.H., Jordan, R.C., 1963. The long term average performance of flat plate solar energy collectors. Solar Energy 7, 53–74.

Moshfegh, B., Sandberg, M., 1998. Flow and heat transfer in the air gap behind photovoltaic panels. International Journal of Renewable and Sustainable Energy Reviews 2, 287–301.

Ong, K.S., Chow, C.C., 2003. Performance of a solar chimney. Solar Energy 74, 1–17.

Prasad, M., Chandra, K.S., 1990. Optimum tilt of solar collector for maximum natural flow. Energy Conversion Management 30, 369–379.

Raman, P., Mande, S., Kishore, V.V.N., 2001. A passive solar system for thermal comfort conditioning of buildings in composite climates. Solar Energy 70, 319–329.

Rodrigues, A.M., Canha da Piedade, A., Lahellec, A., Grandpeix, J.Y., 2000. Modelling natural convection in a heated vertical channel for room ventilation. Building and Environment 35, 455–469.

Sànchez, M.M., Lucas, M., Martínez, P., Sànchez, A., Viedma, A., 2003. Climatic solar roof: an ecological alternative to heat dissipation in buildings. Solar energy 73, 419–432.

Sandberg, M., Moshfegh, B., 1998. Ventilated-solar roof air flow and heat transfer investigation. Renewable Energy 15, 287–292.

Sukhatme, S.P., 1984. Solar Energy: Principles of Thermal Collection and Storage. McGraw-Hill, New Delhi, pp. 58–82.

VDI-Wärmeatlas, 1991. VDI-Verlag GmbH, Dusseldrof, pp. Db15-Db28, Fc1-Fc3, Fd1-Fd4.

Vlachos, N.A., Karapantsios, T.D., Balouktsis, A.I., Chassapis, D., 2002. Design and testing of a new solar tray dryer. Drying Technology 20, 1243–1271.

Ziskind, G., Dubovsky, V., Letan, R., 2002. Ventilation by natural convection of a one-story building. Energy and Buildings 34, 91–102.